Ion cyclotron resonance heating system in the RT-1 magnetospheric plasma

Ion Cyclotron Resonance Heating System in the RT-1 Magnetospheric Plasma

M. Nishiura[1], Y. Kawazura[1], Z. Yoshida[1], N. Kenmochi[1], Y. Yano[1], H. Saitoh[1], M. Yamasaki[1], T. Mushiake[1], A. Kashyap[1], N. Takahashi[1], M. Nakatsuka[1], A. Fukuyama[2]

[1]Graduate School of Frontier Sciences, The University of Tokyo, Chiba 277-8561, Japan

[2]Department of Nuclear Engineering, Kyoto University, Nishikyo-ku, Kyoto 615-8540, Japan

E-mail contact of main author: nishiura@ppl.k.u-tokyo.ac.jp

Abstract.

We have developed an ion cyclotron resonance of frequencies (ICRF) heating system for the Ring Trap 1 magnetospheric device. We excite slow waves from the polar region of the dipole magnetic field. The target helium plasma is produced by electron cyclotron heating. The electrons comprise high-temperature (>10 keV) and low-temperature (<100 eV) components with both typically exhibiting the densities of same order of magnitude. The ICRF heating causes an increase in the ion temperatures and toroidal flow velocities in the core plasma region. We observe appreciable temperature differences between the different ion species (main He^{+} and impurity C^{2+}), suggesting a strong influence of the charge-exchange loss due to which the bulk ions remain relatively cold (~20 eV) compared to the impurity ions (~40 eV). By

developing an electro-optical measurement system, we have measured the local wave electric field in the plasma.

1. Introduction

The Ring Trap 1 (RT-1) device is a laboratory magnetosphere generated by a levitated superconducting ring magnet. Naturally-made magnetospheres, which are ubiquitously created in the Universe, exhibit stable and often high-beta confinement by a simple dipole magnetic field. The strong inhomogeneity of the magnetic field gives rise to various interesting phenomena that highlight the unique properties of the magnetospheric confinement in comparison to that in tokamaks or stellarators. We observe the self-organization of a high-beta plasma clump with a steep density gradient. In addition, a peaked density distribution is spontaneously generated through the up-hill diffusion [1-4]. The presence of confined particles in a dipole field is well-supported by numerical simulations [5]. The up-hill diffusion driven by low-frequency fluctuations that conserve the magnetic moments is accompanied by the betatron effect, resulting in the preferential heating of the perpendicular temperatures [6]. The multi-chord spectroscopic measurement reconstructs the spatial distributions of the ion temperatures (perpendicular $T_\perp$ and parallel $T_\parallel$ components), where $T_\perp$ and $T_\parallel$ are approximately equal to 30 eV and 10 eV, respectively; both of these increase toward the core region. The cold electron temperature T_{ec} is approximately 60 eV. By examining the energy balance model, we separated spontaneous heating power due to the betatron effect from auxiliary heating.

Although the stable high-beta (~1) confinement in magnetospheric plasmas was successfully demonstrated with high-temperature electrons (T_e >10 keV), the heating of the ions has been challenging. The use of the ICRF system is motivated by the need to increase the ion temperature and achieve the high ion beta (~10%). Based on the theoretical results described

by Yoshida *et al*. in Ref. [4], the ion diamagnetism causes a nonlinear strong ion flow that leads to the improvement of plasma confinement. As the first step, we considered to observe the signature of the ion heating by the ICRF heating in the RT-1 plasmas. In the future work, we will optimize the heating efficiency of the ICRF system and to extend the comprehensive understanding of the wave physics in plasmas to the operation region.

The ICRF heating was studied in tokamaks stellarators and linear machines for plasma and fusion research. Because the beach heating scheme exciting a left-hand polarized slow wave [7-11] is applicable to the magnetospheric plasma, we have developed an ICRF heating system for active ion heating in the RT-1. The dipole-field system has unique properties; i.e., the magnetic field only has the poloidal component with the field strength varying strongly along the field lines, and the curvature of the magnetic fields is opposite to that found in the usual toroidal systems. These features require a novel approach for the ion heating in a magnetospheric plasma device. In the RT-1, an antenna is located at the interior high-field side of the device (B ~ 0.52 T) and excites a slow wave propagating toward the resonance region (B ~ 0.13 T) for a magnetic beach heating scheme. We designed both a ∩ shape antenna and a double-loop antenna. The antennas were optimized using the TASK/WF2 code to maximize the wave absorption of the ions. Based on the simulation results, for the electron density of n_e > ~10^{17} m^{-3}, the double-loop antenna yields a higher absorption, while the ∩ shape antenna is better for n_e < ~10^{17} m^{-3}. The ion temperature was increased in helium plasmas by using the ∩ shape antenna. However, the heating effect is observed in the limited operation regime [12].

This paper describes the ICRF heating experiments using the double-loop antenna and their detailed results obtained for the magnetospheric plasmas.

2. Plasma production and ICRF heating in RT-1 magnetospheric plasmas

The superconducting levitation magnet inside the vacuum vessel is levitated by the lifting magnet located outside the vessel. The levitation magnet produces the dipole fields for the confinement of the magnetospheric plasmas. Figure 1 shows the top and cross sectional views of the RT-1 system. The plasma experiments were performed using a levitated magnet (unless otherwise noted). Electron cyclotron (EC) resonance heating produces and sustains the plasmas. The electromagnetic waves for the EC heating are introduced into the vacuum vessel from an 8.2 GHz klystron through two transmission lines of waveguides. The full injection power is 25-kW per line (total of 50 kW).

The double-loop antenna and the poloidal cross-section of the RT-1 are shown in figure 2. The ∩ shape antenna described in [12] is replaced by the newly designed double-loop antenna. The double-loop antenna is located at the interior high-field side and outside the last closed flux surface (LCFS). The ion cyclotron layers are overlaid on the magnetic field lines produced by the levitation magnet. The double-loop antenna is connected to the radio frequency (RF) power supply through the matching circuit and the nominal output is 10 kW in the 0.8–3 MHz frequency range. The other end of the antenna is connected to the ground potential. The lower and upper loop antennas are made of the stainless steel (SUS304) with the radii of 150 and 235 mm, respectively. A single rod with the length of 62 mm joints the two loops in series.

The TASK/WF2 code [13] was used to design and optimize the locations of the two loop antennas for the efficient absorption of the ions in the ion cyclotron layer. The double-loop antenna is located at the higher field side compared to the ion cyclotron resonance layers targeted for H^+, D^+, He^+, and He^{2+}. With the exception of the impurity C^{2+}, the slow wave excited at the antenna position can propagate toward the resonance layers for ion heating. Figure 3 shows the dependence of the absorbed power P_{abs} for He^+ and impurity C^{2+} normalized by

that for the electrons on the electron density for the double-loop antenna. The levitation magnet, the vacuum vessel, and the center stack were modeled with two dimensional conductor boundaries in TASK/WF2 simulation. Three species of electrons, bulk He^+, and impurity C^{2+} exist in the plasma. The electron density was assumed to be a peaked profile as a function of magnetic flux, and the edge electron density was set to be 10^3 times lower than the electron density at the peak. The results of our simulations showed that the input power is mainly absorbed by the bulk He^+. Therefore, the absorbed power to the electrons is almost two orders of magnitude lower than the bulk He^+ and that absorbed by the impurity C^{2+} is much lower. Under the fixed electron density of 10^{17} m^{-3}, in the RF frequency from 0.8 to 3 MHz, the lower RF frequency tends to exhibit better absorption toward He^+. At more than 3 MHz, the absorption by the electron becomes greater than that by He^+. The simulation results reveal the feature of slow wave heating and show that the spatial relation between the lower loop antenna and the ion cyclotron layer of He^+ is dominant. We expect that compared with the former ∩ shape antenna [12], the new antenna improves the efficiency of the slow wave excitation and absorption by the ions for the electron densities higher than 10^{18} m^{-3}.

The RF electric fields of the excited waves in the MHz range were measured in air and plasmas and compared to the results of the simulation performed using the TASK/WF2 code [14]. In air, we obtained a good agreement between the measurement and the simulation. Conversely, in plasmas, the localized RF electric field was observed outside the LCFS, with a steep decrease inside the plasmas. The observed field has not yet been explained by the simulation results.

3. ICRF heating and concomitant phenomena in RT-1

Figure 4 shows the typical discharge waveforms in the ICRF heating experiments. The 8.2-GHz EC heating with 8 kW started at t = 0.975 s and sustained the target plasma for ICRF heating. The helium working gas was introduced into the vacuum vessel with the pressure of 2.2 mPa. The local electron β is converted from the equilibrium analysis of the Grad–Shafranov equation and the measured magnetic field profile as is described in [15]. The ICRF heating turned on at t = 1.03 s and lasted up to t = 1.94 s, before the termination of the target plasma. At the onset of the ICRF heating, a steep drop of the electron density was observed in all interferometer channels. Because a higher electron density in front of the antenna increases the ion heating efficiency according to the TASK/WF2 simulation, the decrease would make the ion heating efficiency worse. At t >1.5 s, the produced plasma remained stable, and the net RF input power dropped to ~6 kW. The drop of the RF power is due to the mismatching of the antenna impedance caused by the decrease in the electron density. The line averaged electron densities were 5.5×10^{16} m^{-3} for the core chord (IF1) and 7.8×10^{15} m^{-3} for the edge chord (IF3).

Upon the application of the ICRF power of 6 kW at the frequency of 2 MHz, the ion heating effect was measured by multichord spectroscopy (scanning and some fixed channels) [6] that resolves the radial profiles of ion temperatures shown in figure 5 and the toroidal flow velocities shown in figure 6 on the equatorial plane Z = 0 m. The appreciable increase in the ion temperature was observed for He II from 12 to 20 eV and for impurity C III from 20 to 45 eV at R ~ 0.6 m. As indicated figure 2, the double probe (DP) is scanned vertically to obtain the electron temperature at the edge region T_e^{edge}. The ICRF heating increases T_e^{edge} by only a few eV, while it decreases the electron density. The pump out of the electron density was also observed at the peripheral chord R = 0.7 m (IF3). The measured data and the model profile

function reconstructed the electron density profile in the RT-1 magnetospheric plasma. Although this method is similar to the methods used in previous work [1, 2, 16], we here combined three interferometer chords and the edge probe measurement (Z ~ 0, R > ~ 0.9 m) to obtain a more accurate reconstruction. The electron density is reduced dramatically at the high-field side between the levitated coil and the centre stack as shown in figure 7. This result indicates that the passing electrons along with the magnetic field are lost near the magnetic pole and that the decrease in the electron density near the double-loop antenna may change the wave propagation and absorption efficiency. The peak density and its position at Z = 0 m almost had the same values. Evaluating the energy balance with the measured temperatures of the ions and the cold electrons, we found that the different temperatures of C III and He II are due to the charge-exchange loss (the characteristic times for charge exchange $\tau_{cx}^{C^{2+}} \sim 250$ ms and $\tau_{cx}^{He^{+}} \sim 0.8$ ms) with the neutral background gas. This is, because the dominant He^{2+} ions exist at $T_{ec} = 50$ eV and working gas pressure of 1 mPa; thus, the state of He^{+} monitored in the case of figure 4 is "burn through" to the higher ionizing state He^{2+} or "charge exchange loss" to the neutral He before being thermalized by the electrons ($\tau_{th}^{He^{+}} \sim 100$ ms).

In a magnetospheric plasma, nonlinear spontaneous flow is expected by ion pressure driven component theoretically [4]. We expect that the ion pressure driven flow improves the plasma confinement. The relation between the transport and ion flow is not unambiguously decomposed to drift- and transport- driven components and was not identified experimentally in a magnetospheric plasma. The main and the impurity ion flows were examined in the same shots of figure 6. The measured flow velocities of He^{+} and C^{2+}, V_i ($i = He^{+}, C^{2+}$) had a peaked profile and $V_i \sim 18$ km/s for both ion species at the peak. The location of the maximum of V_i agrees with that of the ion temperatures. The ICRF heating effect on V_i tends to be small toward the edge region.

The use of a lower helium gas pressure of around 2.2 mPa with a comparable input power of ECRH was used to elucidate the ion heating effect. At the helium gas pressure of 5 mPa, the small increase in the ion temperature was still observed, although the ion temperature of the target plasma was less than 10 eV.

We also observed the increase in the ion temperatures for other gasses such as; hydrogen, deuterium, and hydrogen–helium mixture. In deuterium plasmas with the gas pressure of 11 mPa, the ion temperature of C III increases from 12 to 15 eV at R = 0.645 m. The hydrogen–helium plasmas had an optimal mixture for ion heating with the 20% helium fraction in hydrogen at 10 mPa exhibiting the ion heating from 20 to 45 eV at R = 0.62 m. This experimental result is explained by the model of the eigenmode conversion of the slow wave observed in the linear machine [11]. Because this case does not correspond to that of a magnetospheric configuration, a novel model is required to explain the slow wave heating in two and multi species plasmas relevant to future advanced fusion scenarios.

4. Summary

While the stable high-beta (~1) confinement by a dipole magnetic field has been previously demonstrated with high-temperature electrons (T_e >10 keV) [2], the heating of the ions has been challenging. We have taken the first step toward the development of an ion heating method applicable for the magnetospheric system. We excited slow waves from the antenna located in the polar region of the dipole magnetic field and demonstrated the heating of the ions. We observed the increases in the ion temperatures and their toroidal flow velocities in the core region. The differences in the temperatures among the ion species suggest a strong influence of the charge-exchange loss due to which the bulk ions remain relatively cold (< 20 eV) compared

to the impurity ions. The hydrogen, deuterium as well as helium-hydrogen mixture plasmas also show the increase in ion temperatures by ion heating.

The electro-optic probe system can measure the toroidal component of the electric fields of the RF waves near the LCFS and outside the plasmas of the RT-1 [14]. Using the new approach, we have found that the toroidal electric fields outside the LCFS where the plasma exists are higher than those found by the simulations using the TASK/WF2 code. For the suppression of spurious wave excitations, we would investigate the wave dispersion relation and implement a Faraday shield for the ICRF antenna with the help of the simulation as the next studies. These studies will elucidate clear the excitation, propagation, and absorption of the RF waves in plasmas and improve the ion heating efficiency.

Acknowledgments

This work was supported by JSPS KAKENHI Grant Nos 23224014 and 24360384.

References

[1] Saitoh H, Yano Y, Yoshida Z, Nishiura M, Morikawa J, Kawazura Y, Nogami T, Yamasaki M, *Phys. Plasmas* **21** (2014) 082511.

[2] Nishiura M, Yoshida Z, Saitoh H, Yano Y, Kawazura Y, Nogami T, Yamasaki M, Mushiake T, Kashyap A, *Nucl. Fusion* **55** (2015) 053019.

[3] Yoshida Z, Saitoh H, Yano Y, Mikami H, Kasaoka N, Sakamoto W, Morikawa J, Furukawa M, Mahajan S M, *Plasma Phys. Control. Fusion* **55** (2013) 014018.

[4] Yoshida Z, Mahajan S M, Miushima T, Yano Y, Saitoh H, Morikawa J, *Phys. Plasmas* **17** (2010) 112507.

[5] Sato N, Yoshida Z, Kawazura Y, http://arxiv.org/abs/1510.08571, in 2015.

[6] Kawazura Y, Yoshida Z, Nishiura M, Saitoh H, Yano Y, Nogami T, Sato N, Yamasaki M, Kashyap A, Mushiake T, *Phys. Plasmas* **22** (2015) 112503.

[7] Stix T H, *WAVES IN PLASMAS* (American Institute of Physics, New York, 1992), pp. 342-343.

[8] Hosea J C, Sinclair R M, *Phys. Fluids* **13**, 701 (1970).

[9] Yamaguchi Y, Ichimura M, Ouchi T, Kozawa I, Muro H, Sato S, Fukuyama A, Hojo H, Katano M, Motegi Y, Ohishi J, Murakami T, Sekihara Y, Imai T, *Trans. Fusion Sci. Technol.* **55**, 106 (2009)

[10] Inutake M, Ando A, Hattori K, Tobari H, Makita T, Shibata M, Kasashima Y, Komagome T, *Plasma Phys. Control. Fusion* **49**, A121 (2007).

[11] Roberts D R, Hershkowitz N, *Phys. Fluids B* **4** (1992) 1475.

[12] Nishiura M, Yoshida Z, Yano Y, Kawazura Y, Mushiake T, Saitoh H, Yamasaki M, Kashyap A, Takahashi N, Nakatsuka M, Takase Y, Fukuyama A, *Plasma Fusion Res*. **11** (2016) 2402054.

[13] Fukuyama A, Itoh K, Itoh S-I, *Comput. Phys. Rep*. **4**, 137 (1986).

[14] Nishiura M, Yoshida Z, Mushiake T, Kawazura Y, Osawa R, Fujinami K, Yano Y, Saitoh H, Yamasaki M, Kashyap A, Takahashi N, Nakatsuka M, Fukuyama A, *Rev. Sci. Instrum*. **88** (2017) 023501.

[15] Yano Y, *Experimental Analysis of the Magnetic Field Structure on the High-Beta Plasmas in the Magnetospheric Plasma Device*, PhD thesis, The University of Tokyo (2007).

[16] Saitoh H, Yano Y, Yoshida Z, Nishiura M, Morikawa J, Kawazura Y, Nogami T, Yamasaki M, *Phys. Plasmas* **22** (2015) 024503.

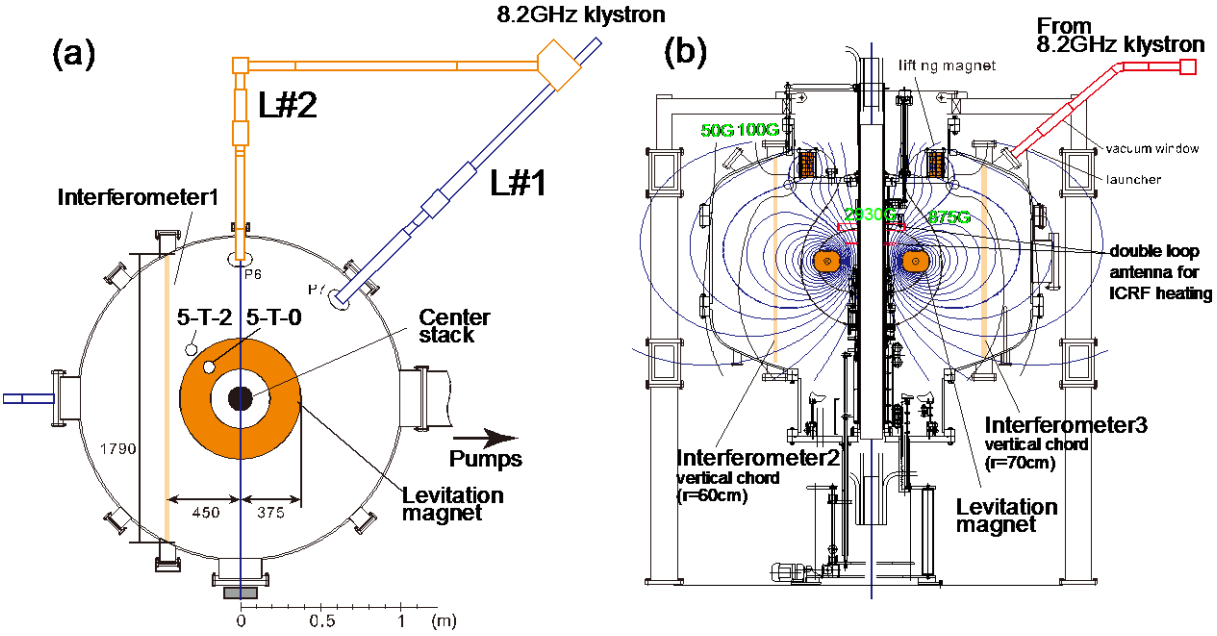

Figure 1. (a) Top and (b) cross sectional views of RT-1. Transmission lines L#1 and L#2 for 8.2-GHz EC heating and three interferometer cords are shown. (c) Double loop antenna used for ICRF heating.

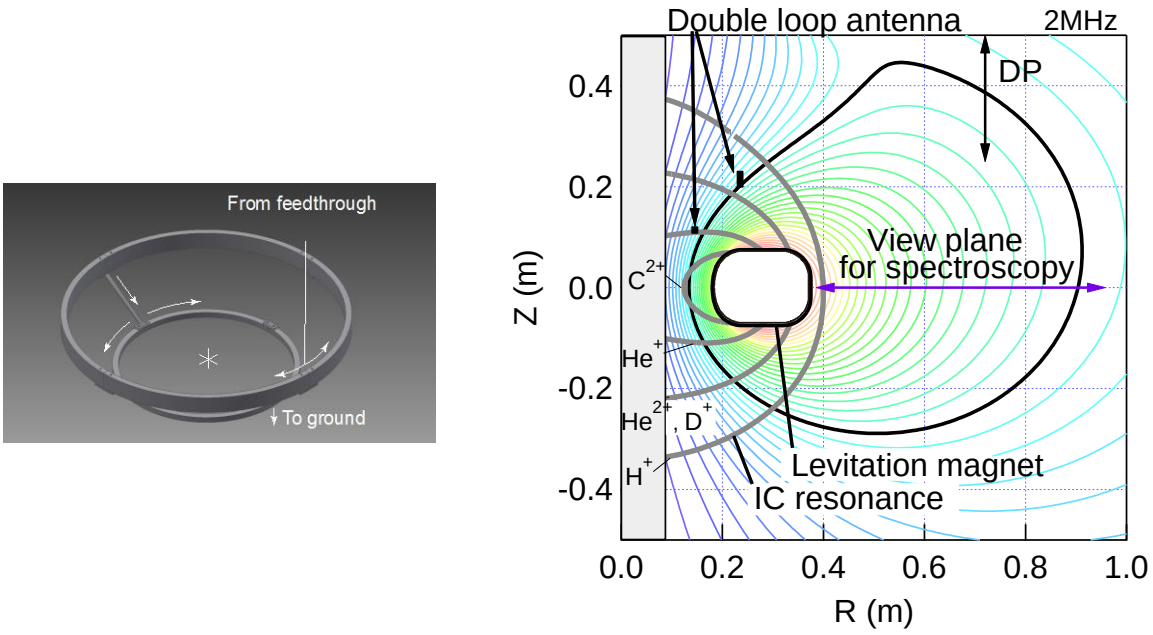

Figure 2. Double-loop antenna and the current direction (left figure). Poloidal cross-section of RT-1 with ion cyclotron resonance layers for main and impurity ions in the case of RF frequency of 2 MHz, and Poloidal field lines. DP is the probe position for edge electron temperature measurement. The position of the double loop antenna is indicated.

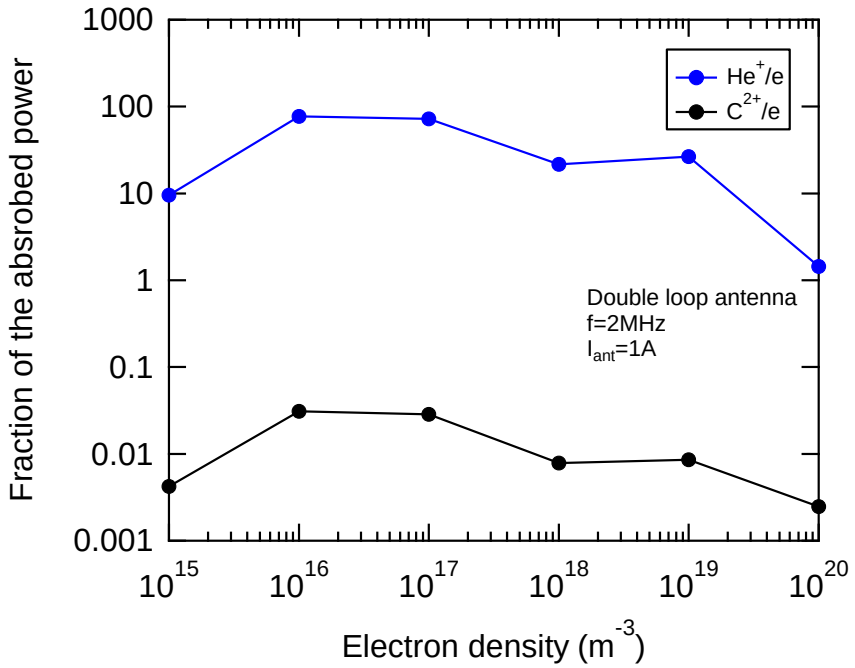

Figure 3. A fraction of the absorbed powers for He^{+} and C^{2+} normalized by that for electron calculated with electrons, helium ions (He^{+}: 99%), and carbon impurities (C^{2+}: 1%) as a function of the electron density in the case of the double-loop antenna. The antenna current of 1 A with the frequency of 2 MHz is applied to the double-loop antenna.

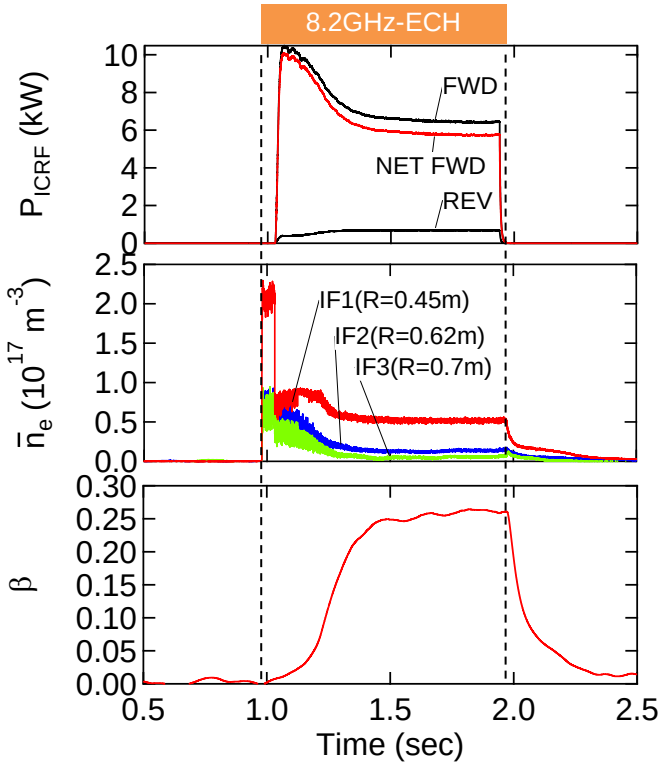

Figure 4. Time evolutions for ICRF forward and reflected powers, line averaged densities $\bar{n}_e$, and local electron β for ICRF heating in high β helium plasma. The target plasma is sustained by 8.2 GHz EC heating. The ICRF power is applied to the double-loop antenna immediately after the start-up of the ECH.

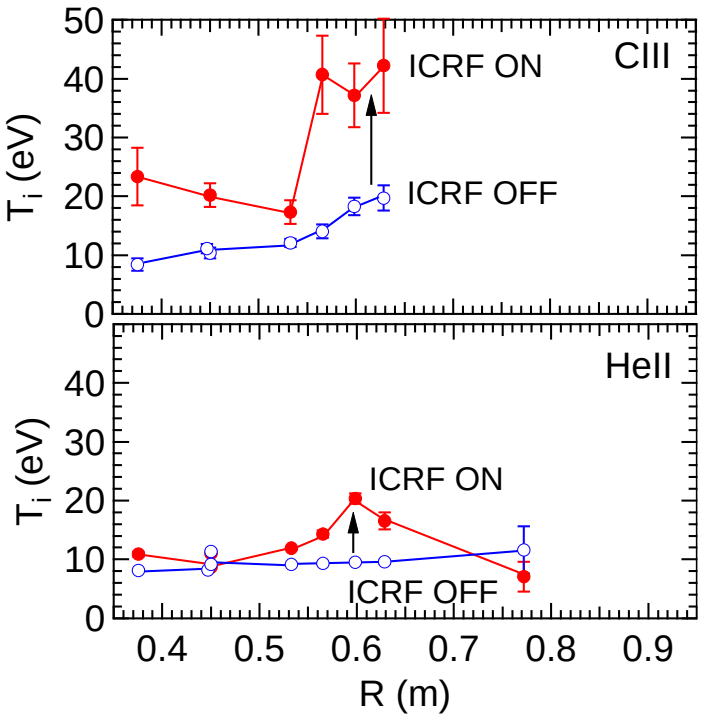

Figure 5. Radial profile of ion temperatures for C III and He II on the equatorial plane of RT-1(see in figure 2) in helium plasmas for the ICRF heating ON (in red) and OFF (in blue). The measured data were accumulated over the time period from 1.5 to 2.0 s.

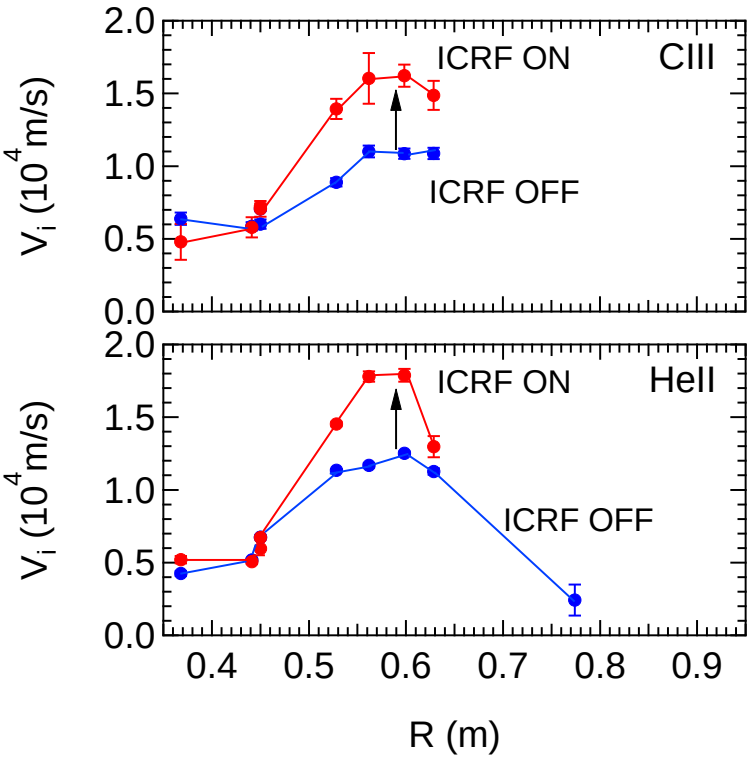

Figure 6. Radial profile of ion flow velocity for C III and He II on the equatorial plane of RT-1 in helium plasmas for the ICRF heating ON (in red) and OFF (in blue). The measured data were accumulated over the time period from 1.5 to 2.0 s.

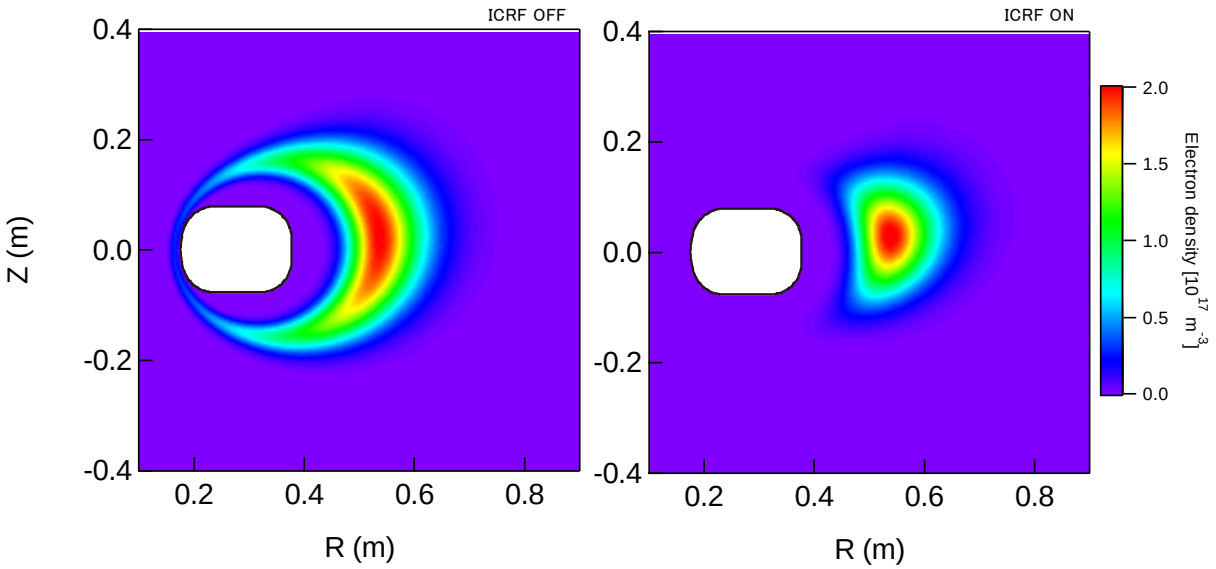

Figure 7. Change in the electron density profiles during the ICRF heating in the RT-1. ICRF heating is turned off (left) and on (right). Density profiles are reconstructed using the data measured by interferometers and DP.